

# A novel biomass-based support (Starbon) for TiO<sub>2</sub> hybrid photocatalysts: a versatile green tool for water purification†

Cite this: *RSC Adv.*, 2013, **3**, 20186

Juan Carlos Colmenares,<sup>\*</sup> Paweł Lisowski and Dariusz Łomot

The average size of the TiO<sub>2</sub> nanoparticles was controlled at around 30 nm on Starbon 800 without using any surfactant, which is attributed to the hydrolysis and condensation (it is also proposed to be a plausible condensation with the carboxylate groups on the carbon surface) of the dissolved titanium(IV) isopropoxide into TiO<sub>2</sub> by ultrasonic waves. As the Starbon in the composites has very good contact with the TiO<sub>2</sub> nanoparticles (there is no Ti leaching after 240 min of photocatalysis, XRF analysis) it enhances the photo-electron conversion (better than Norit and graphene oxide carbons) of TiO<sub>2</sub> by reducing the recombination of photo-generated electron-hole pairs. We have prepared an excellent new hybrid photocatalyst for aqueous phase phenol total mineralization.

Received 15th July 2013  
Accepted 21st August 2013

DOI: 10.1039/c3ra43673j

[www.rsc.org/advances](http://www.rsc.org/advances)

## 1. Introduction

Water pollution by organic compounds is an ever increasing problem globally. Phenol has been selected as the model pollutant due to the fact that it is rated as one of the most toxic organic pollutants in water by United States Environmental Protection Agency. Permissible concentration of phenol in the effluent streams is less than 1 ppm.<sup>1</sup>

Photocatalysis is a good example of green chemistry and occupies a central place in the ecological equilibrium. Titania-based photocatalysis has been identified as a technology playing an important role in solving many of the problems in water purification.<sup>2–4</sup> Apart from the lack of visible light absorption, the application of TiO<sub>2</sub> is restricted by another major obstacle: the post-separation of the semiconductor TiO<sub>2</sub> catalyst after water treatment. The fine particle size of the TiO<sub>2</sub>, together with their large surface area-to-volume ratio and surface energy creates a strong tendency for catalyst agglomeration during the operation. Such particles agglomeration is highly detrimental in views of particles size preservation, surface-area reduction and its reusable lifespan. One way to solve this problem is to load TiO<sub>2</sub> on some supports.

Carbon materials with various properties and forms have been recognized to play an increasingly important participation in heterogeneous catalysis processes as an adsorbent, catalyst support, or even as catalyst on its own. Most of these (*e.g.*, carbon fiber,<sup>5</sup> carbon nanotubes,<sup>6</sup> graphene<sup>7a–c</sup>) have been combined with titania to increase efficiency in heterogeneous

photocatalysis. The high adsorption capacity of carbonaceous materials supports will be a remarkable factor responsible for concentrating the organic contaminant around the supported TiO<sub>2</sub>. After accumulation of the organic over the carbon phase, the driving force for surface diffusion is the gradient on surface concentration between the two phases. To achieve effective transfer, there must be a close contact interface between the two solid phases. In such a way, the organic is transferred from the carbon support to the supported TiO<sub>2</sub> and then undergoes immediate photocatalytic degradation. It can be shown that different synergy factors are obtained for different carbon supports, suggesting that the properties of the carbon phase may play a significant role on the photoefficiency of TiO<sub>2</sub>. A complete review on the use of carbonaceous materials in heterogeneous photocatalysis is already published.<sup>8</sup>

Classical active carbons (AC) are the most frequent used materials in heterogeneous photocatalysis and their preparation generates microporous materials. Industrial use of such materials is limited in applications including catalysis, electrochemistry, fuel cells, biomedical devices and hydrogen storage, partially due to the requirement for tuneable, mesoporous carbon materials. Routes to such materials are not easily accessible, resource and process intensive and ultimately expensive from an industrial viewpoint. Therefore, synthetic approaches (*e.g.* inexpensive green, non-resource and process intensive, *etc.*) are still required which produce largely mesoporous characteristics with chemically active surfaces, that may be produced in a facile manner, allowing tuneability over all these features.

Lately, researchers from the University of York in United Kingdom (Professor James H. Clark research group) have been synthesized (without the need for a templating agent), patented and commercialized under the trademark name “Starbon®” a

*Institute of Physical Chemistry PAS, Kasprzaka 44/52, 01-224 Warsaw, Poland. E-mail: jcarloscolmenares@ichf.edu.pl*

† Electronic supplementary information (ESI) available. See DOI: 10.1039/c3ra43673j

completely new family of porous carbon-based materials derived from cheap biomass feedstock.<sup>9a-e</sup> The resulting carbon-based materials (Starbon family) are highly porous, mechanically and thermally (100–900 °C) stable. The stability of these polysaccharide-derived mesoporous materials at temperatures below 700 °C leads to porous carbonaceous materials with tuneable surface, textural and morphological properties, dependent on the carbonization temperature employed and the polysaccharide used as precursor. This process is gentle and provides the opportunity to produce a whole range of mesoporous carbon-based materials from starch to activated carbon, including amorphous oxygen containing carbons that have many applications such as catalysis,<sup>10a-g</sup> and adsorption.<sup>11</sup> The application of these biomass-based carbon materials has not yet been investigated in heterogeneous photocatalysis. Starbons materials can offer to heterogeneous photocatalysis an enormous potential to prepare novel hybrids TiO<sub>2</sub>-based photocatalysts with interesting properties due mostly to the different controlled functionalities of these biomass-based supports.

Herein we report a novel approach of preparation of nanostructured TiO<sub>2</sub> supported on Starbon-based mesoporous carbon materials and its potential application as photocatalyst for aqueous phase total mineralization of phenol under mild conditions.

## 2. Experimental section

### 2.1 Chemicals and materials

All reagents were used as received without further purification. Titanium(IV) isopropoxide (TTIP > 98%, Acros organics) was used as a precursor of titanium dioxide. Phenol (99%, Alfa Aesar) has been selected as the model pollutant.

Carbonaceous materials: NORIT (activated carbon NORIT SX 2, POCH), GO-graphene oxide (Ref. GO.M.10.21-1, Nanoinnova Technologies SL, Spain), STARBON (Starbon 800, Sigma-Aldrich).

### 2.2 Preparation of hybrid TiO<sub>2</sub>-based carbonaceous materials

For our studies three photocatalysts were prepared. A simple, ultrasound-assisted wet impregnation method was applied to synthesize these materials.<sup>12a,b</sup>

The preparation (surfactant-free synthesis) of hybrid TiO<sub>2</sub> based carbonaceous materials (GO, NORIT, STARBON) was conducted as depicted in Fig. 1: as a first step the above-mentioned carbonaceous materials are subjected to thermal treatment in a furnace at 400 °C, heating rate of 3 °C min<sup>-1</sup> for 5 h in an oxygen-deficient atmosphere (static air). Graphene Oxide (GO) was treated with lower heating rate (1 °C min<sup>-1</sup>) due to the very high loss of mass that we observed during this pretreatment. Then 1.3 g of the carbonaceous material was added into a solution of titanium tetraisopropoxide (1.3 cm<sup>3</sup>, 4.3 mmol TTIP) in isopropanol (total volume ratio of TTIP : isopropanol was 1 : 40) and the whole mixture was sonicated for 60 minutes (ultrasonic bath, frequency 35 kHz, 560 W, Sonorex Digitec-RC, Bandelin). Then, the solvent was

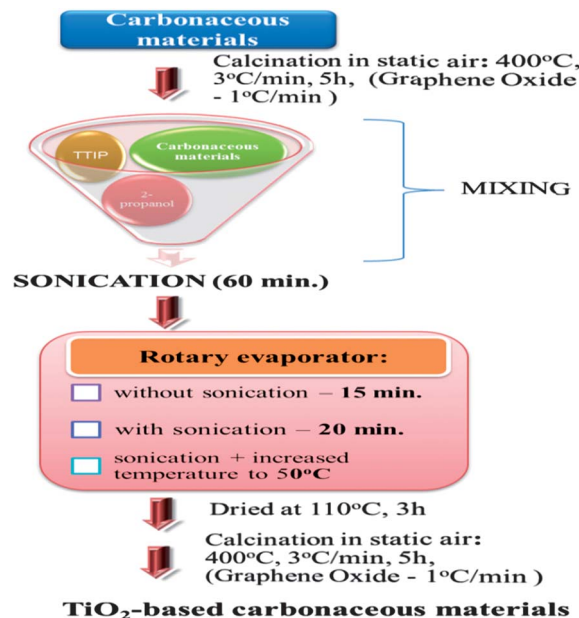


Fig. 1 Synthesis procedure of hybrid TiO<sub>2</sub>-based carbonaceous materials using ultrasound-assisted wet impregnation method.<sup>12a,b</sup>

removed using a rotary evaporator assisted by sonication (ultrasound bath was used instead of water bath).<sup>12a,b</sup> The powder material was further dried for 3 h at 110 °C and subsequently after drying was calcined in a furnace at 400 °C, heating rate of 3 °C min<sup>-1</sup> for 5 h in an oxygen-deficient atmosphere (static air). The content of TiO<sub>2</sub> nanoparticles on the supports was adjusted to 25 wt% (15 wt% of Ti). The final samples were denoted as 15Ti/STARBON, 15Ti/NORIT and 15Ti/GO. A commercial TiO<sub>2</sub> Evonik P25 was also used for comparative purpose.

Schematic picture on the plausible mechanism of TiO<sub>2</sub>-STARBON hybrid material formation (it could be possible for other carbonaceous supports) is presented in Fig. 2. It is believed that the carboxylic acid groups can be formed on the surface after initial thermal treatment at 400 °C under an oxygen-deficient atmosphere. Then, each carboxyl acid group acts as an individual nucleation site for titania formation which is possible under hydrolysis and condensation reactions promoted by sonication. Finally, the hybrid material (TiO<sub>2</sub>-STARBON) is consolidated after thermal treatment at 400 °C.

### 2.3 Photocatalytic activities

All catalytic reactions were performed in a Pyrex cylindrical double-walled immersion well reactor with a total volume of 450 mL. The bath reactor was stirred magnetically to obtain a homogenous suspension of the catalyst. A medium pressure 125 W mercury ( $\lambda_{\text{max}} = 365 \text{ nm}$ ), supplied by Photochemical Reactors Ltd. UK (Model RQ 3010) was placed inside the glass immersion well as light irradiation source. The reaction temperature was established at 30 °C. Phenol solution (50 ppm) was prepared in Milli-Q water. Experiments were carried out from 150 mL of the mother solution and 1 g L<sup>-1</sup> of catalyst concentration was used after previous optimization. All reactions

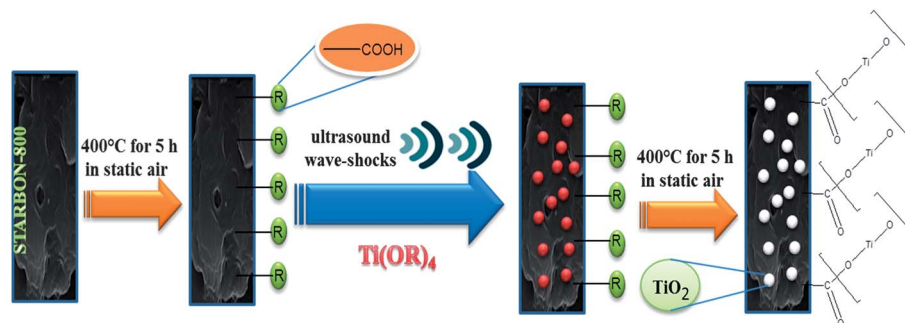


Fig. 2 Schematic illustration of the plausible mechanism of the formation of  $\text{TiO}_2$ -Starbon hybrid material using ultrasound-assisted wet impregnation.

were carried out under ambient air (no oxygen bubbling conditions). Approx. 2 mL of samples were periodically taken from the photoreactor at specified times and filtered through 0.2  $\mu\text{m}$ , 25 mm nylon filters in order to remove photocatalyst. Phenol degradation was measured, after external standard calibration, by HPLC (Waters HPLC Model 590 pump), equipped with a PDA detector. Separation was performed on a XBridge™ C18 5  $\mu\text{m}$  4.6  $\times$  150 mm column provided by Waters. The mobile phase was Milli-Q water-methanol (65 : 35 v/v) mixture with 0.1% of  $\text{CF}_3\text{COOH}$  at a flow rate of 1  $\text{mL min}^{-1}$ . The injection volume was 10  $\mu\text{L}$ . Blank experiments were performed in the dark as well as with illumination and no catalyst, without observable change in the initial concentration of phenol in both cases.

### 3. Results and discussion

As shown in Fig. 3, the 15Ti/STARBON sample shows only the formation of  $\text{TiO}_2$  anatase phase nanoparticles (major peaks: 25.3°, 37.9°, 48.0°, 54.1°, 55.0°, 62.7°). 15Ti/NORIT contains two titania phases, anatase and rutile, in practically the same quantities (45% and 55%, respectively, Table 1). It should be noted the high selectivity to produce anatase is only possible on the Starbon surface which demonstrates the affinity of this carbonaceous support, under our synthetic conditions, to selectively produce anatase (the highest photocatalytically active titania phase). Crystallite sizes for these samples were close each other (30 nm anatase for 15Ti/STARBON and 22.4 nm anatase

and 24.6 nm rutile for 15Ti/NORIT, Table 1) reason why is difficult to discuss on quantum size effect. In the case of graphene oxide-based titania material (15Ti/GO), it can be hardly seen (Fig. 3) the formation of a very broad peak from the  $2\theta$  angle position of anatase, this broad peak on GO can be explained by the absence of crystallization of anatase phase but also it can be suggested a good anatase dispersion on GO surface.

The X-ray analysis also suggests that the heat treatment at 400 °C is sufficient to induce the anatase phase formation in the carbon structure especially for Starbon-based material. It is known that the adsorptive affinity of anatase for organic compounds is higher than that of rutile<sup>43</sup> and anatase exhibits lower rates of recombination electro-hole in comparison to rutile due to its 10-fold greater rate of hole trapping.<sup>14</sup>

The isotherms (Fig. 4a) are of type IV, which is typical for mesoporous materials.<sup>15</sup> 15Ti/STARBON shows a significant high surface area and pore volume as a result of well-developed mesoporosity ( $d_p = 17$  nm) compared to the other catalysts with the same titanium content. The resulting high porosity gives a higher reaction rate (Table 3), due to the high level of interaction of the reactants with the photocatalyst active site. Branch of adsorption and desorption isotherms on all graphs were differently. In the case of 15Ti/NORIT there was no characteristic hysteresis loop which can be seen on the reduced surface area of the catalyst compared with the pure form of the support (results not shown). This may be due to agglomeration of the particles on the catalyst surface or the pores closing during the calcination of the above-mentioned catalyst. Comparing the specific surface area of the catalysts it can be seen that the biggest reduction in the surface area is for 15Ti/NORIT (more than 7 fold) relative to the pure support (Table 2). 15Ti/STARBON and 15Ti/GO are comparable and the surface area of pure carbonaceous material has decreased by 1.6 and 1.3 fold, respectively. 15Ti/STARBON exhibited the highest BET surface area of the materials, 367  $\text{m}^2 \text{g}^{-1}$  and the biggest pore size (17 nm), characteristic of well-defined mesopores material (Table 2). The obtained high porosity ensures enhanced reaction rates due to the high level of interaction of the reactants with the active sites (better phenol diffusion through the pores and then degradation). The relatively large surface area is favorable for an excellent photocatalytic performance. Fig. 4b shows the pore size distribution curve calculated from the adsorption isotherms of nitrogen branch. It can be seen that the

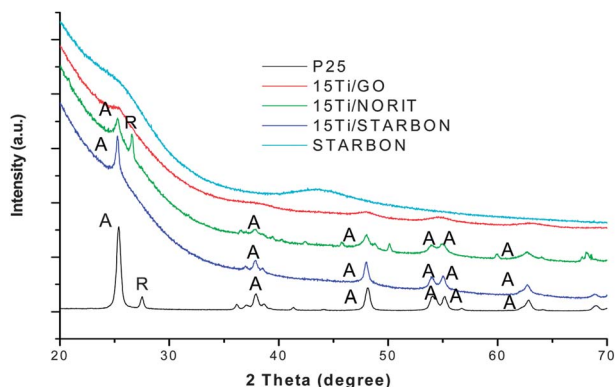
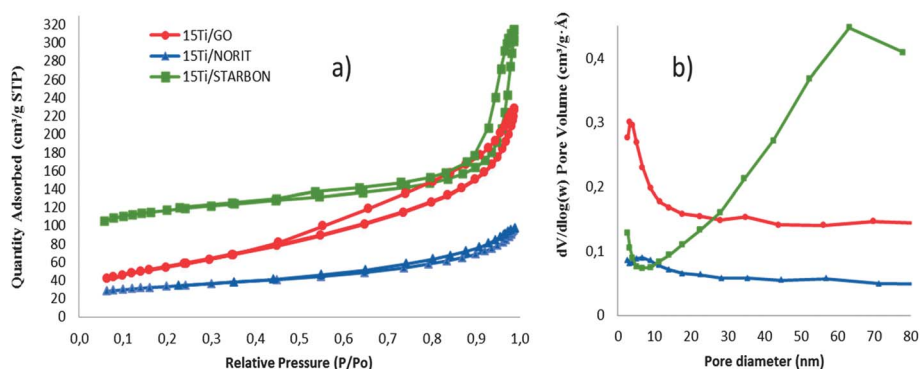


Fig. 3 X-ray diffraction (XRD) pattern for carbon-based photocatalysts.

**Table 1** Summary of the structural and optical features of the photocatalytic systems

Material	XRD		UV-Vis	
	Crystallite size (nm)	Crystal phase (%)	$E_{\text{gap}}$ (eV)	Absorption threshold (nm)
15Ti/GO	Amorphous phase	Amorphous phase	2.61	475
15Ti/NORIT	22.4	Anatase (45) Rutile (55)	2.17	571
15Ti/STARBON	30	Anatase (100)	Difficult to measure	Difficult to measure

**Fig. 4** Nitrogen adsorption–desorption isotherms and pore size distribution plots for 15% Ti on STARBON, NORIT and GO (a and b, respectively).**Table 2** Summary of the textural characteristics of the photocatalytic systems. Specific surface area ( $S_{\text{BET}}$ ), cumulative pore volume ( $V_p$ ), pore mean diameter ( $d_p$ ) as determined from the adsorption branch

$N_2$ -isotherms	GO		NORIT		STARBON	
	15Ti	Pure	15Ti	Pure	15Ti	Pure
$S_{\text{BET}}$ ( $\text{m}^2 \text{g}^{-1}$ )	198	271	111	798	367	610
$V_p$ ( $\text{mL g}^{-1}$ )	0.35	0.12	0.12	0.41	0.34	0.19
$d_p$ (nm)	8	8	9	7	17	18

**Table 3** Apparent rate constant ( $k_{\text{app}}$ ) of phenol degradation for the synthesized photocatalysts

Photocatalyst	$k_{\text{app}}$ (20 min) [ $\text{min}^{-1}$ ]	$R^2$
15Ti/GO	0.0069	0.9625
15Ti/NORIT	0.0065	0.9509
15Ti/STARBON	0.0221	0.9334
(STARBON + P25) – 15%Ti	0.0321	0.9301

pore diameter ranges were in the 7–18 nm which shows a wide distribution of mesopores.

So the large surface area is a requirement, but not a decisive factor. Usually, the photocatalytic activity of amorphous  $\text{TiO}_2$  is negligible (it could be the case of GO-based photocatalyst, Fig. 3 and 8 “red line”), also indicating that crystallinity is another important requirement. As it can be seen in Fig. 3 the crystallinity of anatase for 15Ti/STARBON is much higher than 15Ti/

NORIT, this feature is very important in photocatalysis (the density of defects, which act as recombination centers between photogenerated carriers, decreases with increasing crystallinity) due to the reduction of recombination rate of  $e^- - h^+$  which is of paramount importance in obtaining more stable and active photocatalysts. So a balance between specific surface area and crystallinity is a very important factor in determining the photocatalytic activity of  $\text{TiO}_2$  materials and among tested hybrid photocatalysts this balance is of high level for Starbon-based photocatalyst (Fig. 8, Table 3).

Based on the results of XRF elemental analysis (Fig. 5b, e and h) it can be stated that the main elements, of course not counting carbon “C” from the support, forming part of the catalysts studied are: titanium, calcium and sulfur. In the case of 15Ti/NORIT was additionally detected iron and silicon. SEM images show, especially for 15Ti/STARBON and 15Ti/GO, good ordered shapes with smooth surfaces and without cracks, so may exhibit good adsorption behavior for organic contaminants.

Fig. 6 shows the UV-vis absorbance spectra for photocatalysts: 15Ti/STARBON, 15Ti/NORIT, 15Ti/GO samples and  $\text{TiO}_2$  P25 Evonik (inset). A shift of the absorption edge of 15Ti/GO and 15Ti/NORIT towards longer wavelength region of light is observed (Table 1). In the case of these two samples absorption edge was not as sharp as the edge of Evonik  $\text{TiO}_2$  P25 who showed clear absorption edge at around 375 nm and no absorption in visible region above 400 nm. In our synthesized catalyst samples, we calculated, based on Kubelka–Munk function, band gap of 2.61 and 2.17 eV for 15Ti/GO and 15Ti/NORIT catalysts, respectively (Fig. 7 and Table 1). Unfortunately, the shape of the DR UV-vis spectrum for 15Ti/STARBON did not

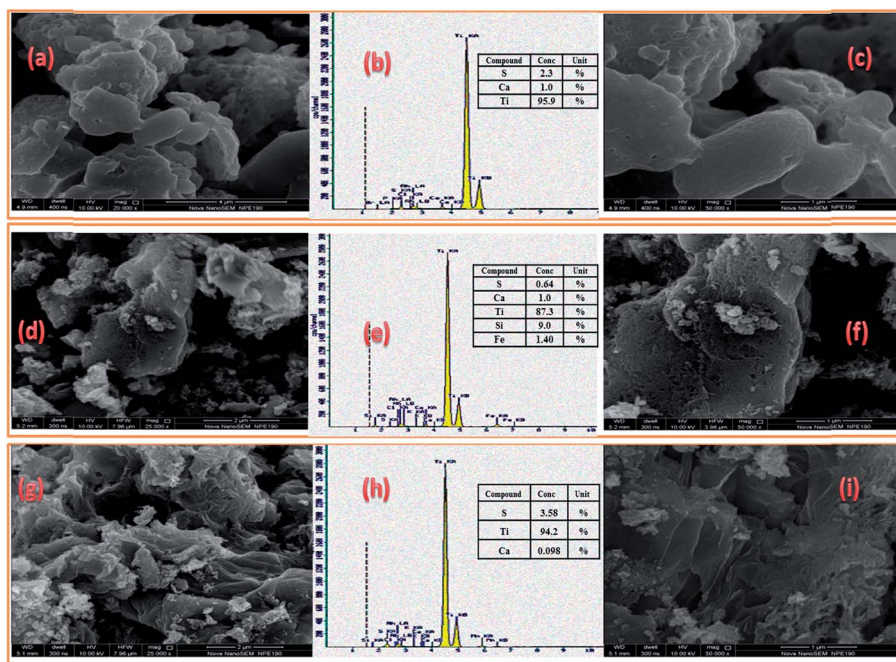


**Fig. 5** SEM images for: 15Ti/STARBON (a and c), 15Ti/NORIT (d and f) and 15Ti/GO (g and i) XRF elemental analysis for: 15Ti/STARBON (b), 15Ti/NORIT (e) and 15Ti/GO (h).

allow us to calculate the band gap ( $E_g$ ) energy for this material. We strongly believe that our prepared materials will show promising photocatalytic activity under visible light.

Phenol disappearance efficiency from water for five independently prepared photocatalysts is shown in Fig. 8. Slight degradation (<5%) of phenol was observed in the absence of a photocatalyst after 240 minutes of illumination (photolysis). Catalyst called STARBON + P25 is the result of mechanical mixing of pure STARBON with commercial Evonik TiO<sub>2</sub> P25, so obtained catalyst contains 25% by weight of TiO<sub>2</sub>. After 240 min of irradiation, the highest phenol disappearance (76%) was achieved with STARBON + P25 sample followed by 15Ti/STARBON (71%), STARBON (68%, mostly due to surface adsorption)

and 15Ti/NORIT sample gave 55% phenol disappearance from water. The lowest grade of disappearance (48%) was achieved with 15Ti/GO photocatalyst.

Table 3 presents the calculated values of apparent rate constant and correlation coefficients ( $R^2$ ) of different photocatalysts after 20 minutes of light irradiation for the aqueous phase phenol degradation. The " $k_{app}$ " have been determined on the basis of linear regression based on  $\ln(C/C_0) = -kt$  function (pseudo first-order reaction). The order of photodegradation efficiency of phenol under UV light is as follows: STARBON + P25 > 15Ti/STARBON > 15Ti/GO  $\geq$  15Ti/NORIT based on  $k_{app}$  (20 minutes) (Table 3). Mixture STARBON + P25 which contains 25% TiO<sub>2</sub> (15% Ti) was 1.4 fold more active than 15Ti/

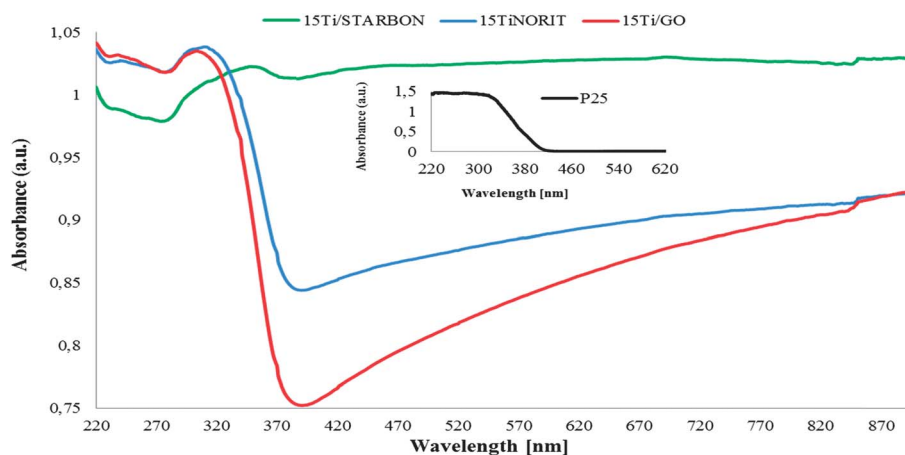


**Fig. 6** Diffuse reflectance UV-visible spectra of catalyst samples: 15Ti/STARBON ("green line"), 15Ti/NORIT ("blue line"), 15Ti/GO ("red line") and TiO<sub>2</sub> P25 Evonik (inset).

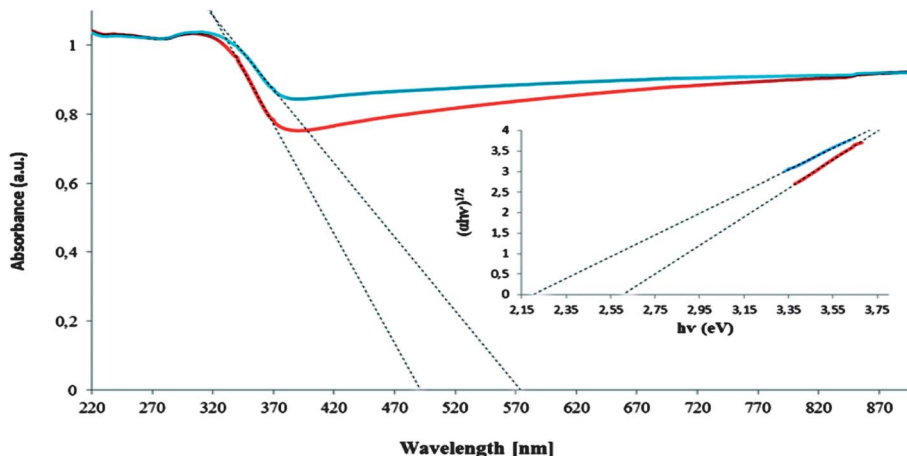


**Fig. 7** Diffuse reflectance UV-visible spectra of catalyst samples: 15Ti/NORIT ("blue line"), 15Ti/GO ("red line") and plot of transformed Kubelka–Munk function versus the energy of the light absorbed for these catalysts (inset).

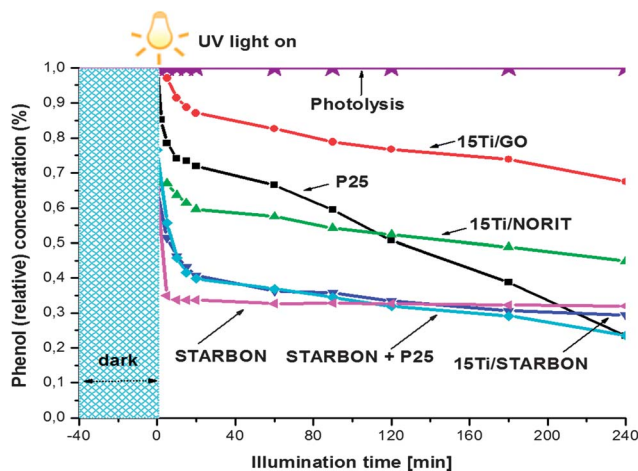


**Fig. 8** Photocatalysts activities in aqueous phase degradation of phenol (reaction conditions: 150 mL of mother solution, 150 mg of photocatalyst,  $C_{\text{phenol}} = 50$  ppm, temperature 30 °C, reaction pressure 1 bar).

STARBON, 4.7 fold of 15Ti/GO and 4.9 fold of 15Ti/NORIT. All results demonstrated that the as-prepared  $\text{TiO}_2$  nanostructured composites with enhanced photocatalytic activity were appropriate for the application in the degradation of organic pollutants (e.g. phenol). The enhanced STARBON-based photocatalyst activity (3.4 fold and 3.2 fold higher than NORIT-based and GO-based photocatalyst, respectively, Table 3) can be ascribed to the enhanced adsorbent activity of the composite system, hybrid interphases ( $\text{TiO}_2 + \text{STARBON}$ ) proximity and the appearance of 100% of high-crystalline anatase phase. Phenol can be adsorbed onto the photocatalyst surface more quickly and degraded there which was confirmed by additional phenol surface extraction experiments<sup>16</sup> (results shown in Table 4). Coating  $\text{TiO}_2$  photocatalyst on the surface of Starbon combines the advantages of both techniques, i.e. on one hand, Starbon works as the support of nanosized  $\text{TiO}_2$  photocatalyst and concentrates the pollutants and intermediates around the  $\text{TiO}_2$ ; on the other hand, the  $\text{TiO}_2$  photocatalyst can destroy effectively the adsorbed

**Table 4** Results of extracting phenol from samples' surfaces after 240 minutes of photocatalysis

Photocatalyst	Amount of phenol extracted from the sample surface [%]
STARBON – Pure	52.9
15Ti/STARBON	3.0
STARBON + P25	8.7

pollutants thus regenerating the Starbon *in situ* (only 3% of the initial concentration of phenol still stayed on Starbon surface after 240 minutes of reaction in comparison with 8.7% for STARBON + P25, Table 4). That means that, in fact 15Ti/STARBON is more active in terms of phenol mineralization (carbon dioxide and water formation) after 240 minutes of illumination (32.4% of phenol is still in water and after extraction from 15Ti/STARBON surface in comparison with 39.2% of phenol for STARBON + P25).

Most phenol content (almost 53%) was extracted from the surface of pure STARBON which confirms the capability of adsorption of this mesoporous carbon material.

As far as photocatalyst stability is concerned, our best photocatalytic system (15Ti/STARBON) was reused three times under the same reaction conditions with the loss of only 5% of phenol degradation after the third cycle (in comparison with the fresh photocatalyst).

## 4. Conclusions

We have demonstrated that the ability of Starbon-800 materials to serve as a solid support to anchor titania nanoparticles (hybrid  $\text{TiO}_2$  photocatalysts) is useful in developing new photocatalysts. Starbon-based mesoporous carbon structures constitute a new class of nanomaterials for  $\text{TiO}_2$  photocatalysts with properties that differ significantly from other forms of carbon-based photocatalysts such as active carbon (Norit) and graphene oxide (GO). Therefore, we demonstrated an enhanced

photocatalytic activity for TiO<sub>2</sub>, when it is dispersed/anchored on ordered Starbon mesoporous carbon material. The improved activity, compared with that of TiO<sub>2</sub>/Norit and TiO<sub>2</sub>/GO, was attributed to the reversible adsorption of phenol on the hydrophobic sites of the Starbon support and the highly dispersed TiO<sub>2</sub> anchored on ordered mesoporous carbon by the ultrasound-induced impregnation method. Another reason cited for the enhanced activity was the formation of pure anatase phase with high crystallinity (reduction of the electron-hole recombination rate) on the Starbon surface. The photochemical properties of mesoporous carbons facilitate modulation of their charge transfer properties and aid in the design of photocatalysts for phenol degradation.

The development of novel hybrid mesoporous photocatalysts (titania on Starbon) with different surface functionalities may open new doors to photocatalysis.

## Acknowledgements

This research was supported by a Marie Curie International Reintegration Grant within the 7<sup>th</sup> European Community Framework Programme. This scientific work was financed from the 2012–2014 science financial resources, granted for the international co-financed project implementation (Project no. 473/7.PR/2012, Ministry of Science and Higher Education of Poland). We also want to extend our thanks to Dr W. Juszczyk and Dr D. Lisovytskiy for XRD and XRF measurements, respectively.

## References

- 1 N. N. Mahamuni and A. B. Pandit, *Ultrason. Sonochem.*, 2006, **13**, 165–174.
- 2 J. C. Colmenares, R. Luque, J. M. Campelo, F. Colmenares, Z. Karpinski and A. A. Romero, *Materials*, 2009, **2**, 2228–2258.
- 3 M. N. Chong, B. Jin, C. W. K. Chow and C. Saint, *Water Res.*, 2010, **44**, 2997–3027.
- 4 J.-M. Herrmann and M. Lacroix, *Kinet. Catal.*, 2010, **51**, 793–800.
- 5 R. S. Yuan, J. T. Zheng, R. B. Guan and Y. C. Zhao, *Colloids Surf., A*, 2005, **254**, 131.
- 6 H. T. Yu, H. M. Zhao, X. Quan and S. Chen, *Chin. Sci. Bull.*, 2006, **51**, 2294.
- 7 (a) S. Morales-Torres, L. M. Pastrana-Martínez, J. L. Figueiredo, J. L. Faria and A. M. T. Silva, *Environ. Sci. Pollut. Res.*, 2012, **19**, 3676–3687; (b) D. Chen, H. Zhang, Y. Liu and J. Li, *Energy Environ. Sci.*, 2013, **6**, 1362–1387; (c) Q. Xiang, J. Yu and M. Jaroniec, *Chem. Soc. Rev.*, 2012, **41**, 782–796.
- 8 J. L. Faria and W. Wang, *Carbon Materials for Catalysis*, ed. P. Serp and J. L. Figueiredo, 2009, ch. 13, pp.481–506.
- 9 (a) V. Budarin, J. H. Clark, J. J. E. Hardy, R. Luque, K. Milkowski, S. J. Tavener and A. J. Wilson, *Angew. Chem., Int. Ed.*, 2006, **45**, 3782–3786; (b) S. Doi, J. H. Clark, D. J. Macquarrie and K. Milkowski, *Chem. Commun.*, 2002, 2632–2633; (c) J. H. Clark, F. E. I. Deswarte, J. J. E. Hardy, A. J. Hunt, F. M. Kerton and K. Milkowski, PCT Patent Application, PCT/GB2004/003276, 2004; (d) K. Milkowski, J. H. Clark and S. Doi, *Green Chem.*, 2004, **6**, 189–190; (e) V. Budarin, J. H. Clark, F. E. I. Deswarte, J. J. E. Hunt, A. J. Hardy and F. M. Kerton, *Chem. Commun.*, 2005, 2903–2905.
- 10 (a) V. Budarin, J. H. Clark, R. Luque and D. J. Macquarrie, *Chem.–Eur. J.*, 2007, **13**, 6914; (b) V. Budarin, J. H. Clark, R. Luque, D. J. Macquarrie, A. Koutinas and C. Webb, *Green Chem.*, 2007, **9**, 992; (c) V. Budarin, J. H. Clark, R. Luque and D. J. Macquarrie, *Chem. Commun.*, 2007, 634; (d) V. Budarin, J. H. Clark, R. Luque, D. J. Macquarrie, K. Milkowski and R. J. White, PCT Int. Appl., WO 2007104798 A2 20070920, 2007; (e) R. Luque, V. Budarin, J. H. Clark and D. J. Macquarrie, *Appl. Catal., B*, 2008, **82**, 157–162; (f) R. Luque, J. H. Clark, K. Yoshida and P. L. Gai, *Chem. Commun.*, 2009, 5305–5307; (g) R. Luque, V. Budarin, J. H. Clark and D. J. Macquarrie, *Green Chem.*, 2009, **11**, 459–461.
- 11 H. L. Parker, A. J. Hunt, V. L. Budarin, P. S. Shuttleworth, K. L. Miller and J. H. Clark, *RSC Adv.*, 2012, **2**, 8992–8997.
- 12 (a) J. C. Colmenares, A. Magdziarza, K. Kurzydowski, J. Grzonka, O. Chernyayeva and D. Lisovytskiy, *Appl. Catal., B*, 2013, **134**, 136–144; (b) J. C. Colmenares, A. Magdziarza, O. Chernyayeva, D. Lisovytskiy, K. Kurzydowski and J. Grzonka, *ChemCatChem*, 2013, **5**, 2270–2277.
- 13 U. Stafford, K. A. Gray, P. V. Kamat and A. Varma, *Chem. Phys. Lett.*, 1993, **205**, 55.
- 14 G. Riegel and J. R. Bolton, *J. Phys. Chem.*, 1995, **99**, 4215.
- 15 S. J. Gregg and K. S. W. Sing, *Adsorption, Surface Area and Porosity*, Academic Press, London, 1982.
- 16 Y. Ao, J. Xu, D. Fu, X. Shen and Ch Yuan, *Colloids Surf., A*, 2008, **312**, 125–130.